Form-Finding and Physical Property Predictions of Tensegrity Structures Using Deep Neural Networks

1st Muhao Chen

Department of Mechanical and Aerospace Engineering
University of Kentucky
Lexington, KY 40506
muhaochen@uky.edu

2nd Jing Qin

Department of Mathematics

University of Kentucky

Lexington, KY 40506

jing.qin@uky.edu

Abstract—In the design of tensegrity structures, traditional form-finding methods utilize kinematic and static approaches to identify geometric configurations that achieve equilibrium. However, these methods often fall short when applied to actual physical models due to imperfections in the manufacturing of structural elements, assembly errors, and material nonlinearities. In this work, we develop a deep neural network (DNN) approach to predict the geometric configurations and physical properties-such as nodal coordinates, member forces, and natural frequencies-of any tensegrity structures in equilibrium states. First, we outline the analytical governing equations for tensegrity structures, covering statics involving nodal coordinates and member forces, as well as modal information. Next, we propose a data-driven framework for training an appropriate DNN model capable of simultaneously predicting tensegrity forms and physical properties, thereby circumventing the need to solve equilibrium equations. For validation, we analyze three tensegrity structures, including a tensegrity D-bar, prism, and lander, demonstrating that our approach can identify approximation systems with relatively very small output errors. This technique is applicable to a wide range of tensegrity structures, particularly in real-world construction, and can be extended to address additional challenges in identifying structural physics information.

Index Terms—tensegrity, form-finding, natural frequencies, deep neural networks

I. INTRODUCTION

The concept of tensegrity is defined by a stable arrangement of compressive (bars or struts) and tensile (strings or cables) elements [1]. Extensive research into tensegrity has revealed several advantages, including its lightweight nature [2], adjustable stiffness [3], and significant morphing capabilities [4]. These attributes have enabled its use in diverse applications such as airfoil design [5], metamaterials development [6], fish robot creation [7], rover innovation [8], tower engineering [9], climbing robot development [10], robotic manipulator [11], and self-assembling modular robots [12]. Consequently, tensegrity has proven to be a versatile foundation for designing novel, lightweight, and deployable structural systems.

Despite the increasing popularity of tensegrity structures, significant challenges persist in determining their geometrical configurations through a process known as form-finding. Early pioneers in tensegrity, i.e., Snelson [13], primarily

The research of J.Q. is supported by NSF grant DMS-1941197.

used regular, convex polyhedra as the basis for exploring new configurations of tensegrity structures. However, physical models indicate that the shape of a tensegrity structure based on specific polyhedra, such as the truncated tetrahedron or the expandable octahedron, deviates from the original polyhedral form [14]. Consequently, proper form-finding methods are crucial for accurately determining the equilibrium configurations of even basic tensegrity structures [15]. Form-finding methods for tensegrity structures have been extensively studied.

Most of the work begins by developing analytical approaches or efficient algorithms to tackle their nonlinear statics. Examples include the force density method [16], dynamic relaxation method [17], Levenberg-Marquardt method [18], and Laplacian matrix based method [19]. However, these methods often encounter limitations when applied to actual physical models. Such limitations typically stem from various practical issues, such as imperfections in the manufacturing of structural elements, assembly errors, and the effects of material fatigue, erosion, and creeping. These factors, along with other unpredictable reactions, are difficult to model analytically, leading to significant discrepancies in the calculated physical properties of real tensegrity structures.

Recently, machine learning has gained significant traction due to its remarkable ability to process large-scale datasets. Several initiatives have been undertaken to apply machine learning to the problem of form-finding in tensegrity structures. For instance, Lee et al. substituted the traditional force density method with deep neural networks that predict element lengths from force densities [20]. Zalyaev et al. developed a machine learning pipeline that includes feature extraction and regression for Tensegrity Form Finding [21]. Additionally, Kim et al. employed a Monte Carlo-based learning algorithm to control the locomotion of tensegrity robots through formfinding [22]. However, very few of them could provide any physical properties of the tensegrity structure other than nodal coordinates. In many applications, physical properties such as tension forces and frequencies are key considerations in tensegrity structure design to ensure structural stability, load distribution, and overall performance. In addition, when dealing with a large number of tensegrity structures within the same category, data-driven approaches, such as DNNs, would be more efficient in simultaneously inferring tensegrity forms and physical properties based on the cable length changes than model-driven methods, such as solving static equilibrium equations. Motivated by these insights, we aim to develop a novel DNN-based modeling framework for predicting aspects of tensegrity form-finding and physical properties, including nodal coordinates, tension forces, and frequencies.

The rest of the paper is structured as follows: Section II introduces the notations and governing equations of tensegrity structures. Section III details the DNN model, including the testing and prediction framework. Section IV examines three case studies involving a tensegrity D-bar, prism, and lander and discusses the results. The paper concludes with Section V, which offers a discussion of the findings and outlines directions for future research.

II. GOVERNING EQUATIONS OF TENSEGRITY STRUCTURES

Before exploring the physics of tensegrity structures, such as equilibrium states affected by changes in string force, forces in all the structural members, and natural frequencies, we introduce the notations and governing equations relevant to any tensegrity systems.

A. Tensegrity Structure Notations

Definition II.1 (Nodal Coordinates). The nodes in a tensegrity structure can be represented in both vector and matrix forms: the vector form is denoted as: $\mathbf{n} = \begin{bmatrix} \mathbf{n}_1^{\mathrm{T}} & \mathbf{n}_2^{\mathrm{T}} & \cdots & \mathbf{n}_{n_n}^{\mathrm{T}} \end{bmatrix}^{\mathrm{T}} \in \mathbb{R}^{3n_n}$, and the matrix form is $\mathbf{N} = \begin{bmatrix} \mathbf{n}_1 & \mathbf{n}_2 & \cdots & \mathbf{n}_{n_n} \end{bmatrix} \in \mathbb{R}^{3 \times n_n}$. Here, n_n represents the total number of nodes, and $\mathbf{n}_i = \begin{bmatrix} x_i & y_i & z_i \end{bmatrix}^{\mathrm{T}}$ corresponds to the x-, y-, and z-coordinates of the i-th node $(i = 1, 2, \ldots, n_n)$.

Definition II.2 (Connectivity Matrices). Connectivity matrices represent the patterns of connections between bars and strings in the nodes of a structure. The matrices for bars and strings are denoted as $C_b \in \mathbb{R}^{n_b \times n_n}$ and $C_s \in \mathbb{R}^{n_s \times n_n}$, where n_b and n_s indicate the total numbers of bars and strings, respectively. For each structure element k connecting nodes n_i and n_j (where i < j), the connectivity matrices include a "-1" at the k-th row and i-th column, a "+1" at the k-th row and j-th column, and zeros elsewhere in the same row. The indices i and j range from l to n_n , and k ranges from l to n_b for bars and l to n_s for strings. The complete connectivity matrix $C \in \mathbb{R}^{n_e \times n_n}$ (with $n_e = n_s + n_b$ representing the total number of structural elements) is formed as $C = [C_b^T \quad C_s^T]^T$.

B. Tensegrity Governing Equations

Theorem II.1 (Tensegrity Statics). The static equilibrium equations for a tensegrity structure, expressed in terms of the nodal vector \mathbf{n} and the member force vector \mathbf{t} , are given by:

$$\boldsymbol{E}_{a}^{T}\boldsymbol{K}\boldsymbol{n} = \boldsymbol{E}_{a}^{T}(\boldsymbol{f}_{ex} - \boldsymbol{g}), \tag{1}$$

$$\boldsymbol{E}_{a}^{T}\boldsymbol{A}_{t}\boldsymbol{t} = \boldsymbol{E}_{a}^{T}(\boldsymbol{f}_{ex} - \boldsymbol{g}), \tag{2}$$

where $K = (C^T \hat{x}C) \otimes I_3$ and $A_t = (C^T \otimes I_3)b.d.(NC^T)\hat{l}^{-1}$ represent the stiffness matrix and equilibrium matrix. Here, \otimes denotes the Kronecker product, and the

operator b.d.(V) converts each column of the matrix V into a block diagonal matrix. The matrix $E_a \in \mathbb{R}^{3n_n \times 3n_a}$ (where n_a is the number of free nodes) serves as an orthogonal index matrix to isolate the free nodes n_a from all nodes n, satisfying $n_a = E_a^T n$. Here, x and x denote the force density and the length of members, respectively, and \hat{v} is a diagonal matrix with the components of vector x along its diagonal.

The proof is given in [23] using the Lagrangian method. Given that K is a function of n, Eq. (1) is nonlinear with respect to n. The process of determining the final configuration from specified loading conditions and an initial configuration can be solved by Algorithm 1.

Theorem II.2 (Tensegrity Modal Information). The modal information of a tensegrity structure can be determined by solving the generalized eigenvalue problem:

$$K_{Taa}\varphi = \omega^2 M_{aa}\varphi, \tag{3}$$

where:

$$\boldsymbol{M} = \frac{1}{6} (|\boldsymbol{C}|^T \hat{\boldsymbol{m}} |\boldsymbol{C}| + \lfloor |\boldsymbol{C}|^T \hat{\boldsymbol{m}} |\boldsymbol{C}| \rfloor) \otimes \boldsymbol{I}_3$$
(4)

$$\boldsymbol{K}_{Taa} = \boldsymbol{E}_a^T \boldsymbol{K}_T \boldsymbol{E}_a, \ \boldsymbol{M}_{aa} = \boldsymbol{E}_a^T \boldsymbol{M} \boldsymbol{E}_a, \tag{5}$$

$$\boldsymbol{K}_T = (\boldsymbol{C}^T \hat{\boldsymbol{x}} \boldsymbol{C}) \otimes \boldsymbol{I}_3 + \boldsymbol{A}_1 \hat{\boldsymbol{E}} \hat{\boldsymbol{A}} \hat{\boldsymbol{I}}^{-3} \boldsymbol{A}_1^T, \tag{6}$$

$$\mathbf{A}_1 = (\mathbf{C}^T \otimes \mathbf{I}_3) b.d. (\mathbf{N}\mathbf{C}^T), \tag{7}$$

where E and A in \mathbb{R}^{n_e} denote Young's modulus and cross-sectional area of all elements, respectively. The variable ω represents the natural frequency of the tensegrity system, and φ is the eigenvector corresponding to the mode shape.

By linearizing the dynamics equation and omitting the external force and damping terms, one can derive the generalized eigenvalue equation, and details are provided in [23].

III. DATA-BASED MODELING BY DEEP NEURAL NETWORKS

In this work, we apply the sequential feedforward DNN in Keras [24], which consists of multiple hidden layers between the input and output layers. Each layer typically applies a nonlinear transformation to its input, allowing the network to learn complex patterns in the data. We aim to use DNN to learn tensegrity forms, which are encoded by the node coordinate information, and the physical properties of tensegrity structures, such as tension forces and frequencies. To be specific, we use $\mathbf{y}=(\mathbf{n}_a,\mathbf{t},\boldsymbol{\omega})$ to denote the solution estimated by DNN and assume that the DNN architecture consists of L+1 layers with the middle L-1 hidden layers. To find the forward solution, the first layer takes the change of cable rest length \mathbf{l}_0 as the input, and the last layer produces the solution \mathbf{y} as the output. Let z_i^ℓ be the value of the i-th neuron at the ℓ -th layer. Then the j-th neuron at the ℓ -th layer has the value as:

$$z_j^{\ell+1} = \sigma_{\ell+1} \left(\sum_{i=1}^{m_\ell} w_{ji}^{\ell+1} z_i^{\ell} + b^{\ell+1} \right), \tag{8}$$

where $\sigma_{\ell+1}$ is the activation function, $w_{ji}^{\ell+1}$ is the weight between the neurons z_j and z_i , and $b^{\ell+1}$ is the bias term at

Algorithm 1: Solutions to the Tensegrity Form-Finding and Physical Properties.

1) Initialization: Given structure initial configuration n^0 , free nodal index matrix E_a , connectivity matrix C, prestress x_0 in the structure members, external force f_{ex} , and equilibrium computational tolerance ϵ and a positive scalar μ , i.e., $\epsilon = 10^{-6}$ and $\mu = 0.1$. 2) Input: the change of rest length $d\mathbf{l}_0$ of the members. 3) Compute rest length of the members $ar{l}_0 = l_0 + \mathrm{d} l_0$, the force density $m{x} = \hat{m{E}}\hat{m{A}}(ar{m{l}}_0^{-1} - m{l}^{-1})$ and the initial stiffness $K|_{n^0}$ and out of balance force: $oldsymbol{f}_a^0 = oldsymbol{E}_a^T (oldsymbol{f}_{ex} - oldsymbol{g} - oldsymbol{K}|_{oldsymbol{n}^0} oldsymbol{n}^0).$ while $||f_a^i|| > \epsilon$ do Compute K_{Taa} , set $\lambda \leftarrow \min\{eig(K_{Taa})\}$. $\tilde{\pmb{K}}_{Taa} = \begin{cases} \pmb{K}_{Taa} + (\mu + |\lambda|) \pmb{I}, \ \lambda < 0, \\ \pmb{K}_{Taa} + \mu \pmb{I}, \ \lambda \geq 0. \end{cases}$ Compute the increment of the nodal displacement: $\mathrm{d} \pmb{n}_a^i = \tilde{\pmb{K}}_{Taa}^{-1} \pmb{f}_a^{i-1}.$ Modify the tangent stiffness matrix: Compute δ from $\begin{cases} \min_{\delta} V, \\ \text{s.t. } 0 < \delta \leq 1. \end{cases}$ Line search method: $\boldsymbol{n}_a^i = \boldsymbol{n}_a^{i-1} + \delta \mathrm{d} \boldsymbol{n}_a^i.$ Compute the out of balance force: $oldsymbol{f}_a^i = oldsymbol{E}_a^T (oldsymbol{f}_{ex} - oldsymbol{g} - oldsymbol{K}|_{oldsymbol{n}^i} oldsymbol{n}^i).$ end while Output: The coordinate n_a at the final state, member

the $(\ell + 1)$ -th layer. One common option for the activation function is the Rectified Linear Unit (ReLU), which sets all negative values to zero and keeps positive values unchanged. Note that the number of neurons at the ℓ -th layer m_{ℓ} can be distinct across layers. Therefore, the output of the (L+1)th layer from the entire network is the desired solution, i.e., $oldsymbol{y} = (z_0^{L+1}, \dots, z_{m_{L+1}}^{L+1}).$ Through the training stage, we intend to obtain the optimal weights and biases to minimize some loss function for the network, e.g., mean squared error (MSE) between the predicted outputs and the actual outputs. Then, a stochastic optimization algorithm such as Adaptive moment estimation (Adam) [25] can be applied in the backpropagation step of DNN to obtain the optimal weights and biases. The prediction accuracy of the learned DNN model for predicting node coordinates and physical properties of specific tensegrity structures can be evaluated through the testing stage.

force vector t, and natural frequency ω from Eq. (3).

IV. NUMERICAL EXPERIMENTS

In this section, we conduct numerical experiments on three types of tensegrity structures, including a D-bar unit, prism, and lander, to justify the effectiveness of the proposed framework in solving form-finding problems. To evaluate prediction accuracy, we use the average MSE over 20 trials to reduce the randomness of the results, i.e., each random test is repeated 20 times. Throughout the experiments, we generate data sets by

applying Algorithm 1 with various selections of rest lengths of the cables. In particular, we focus on a uniform random selection of cable lengths. To standardize data ranges and enhance learning accuracy, we divide the forces and the frequencies by 10^3 N and 10^6 Hz, respectively. We generate five datasets consisting of 1,000, 2,000, 3,000, 4,000, and 5,000 data samples for all the examples. In the DNN, we follow the 80-20 train-test split, i.e., the first 80% of the randomly shuffled dataset is allocated to the training set, with the remainder assigned to the test set.

All the numerical experiments are implemented on Python 3 in a desktop computer with Intel CPU i9-9960X RAM 64GB and GPU Dual Nvidia Quadro RTX5000 with Windows 10 Pro. In addition, a DNN model is built in Keras [24], which uses the ReLU and Adam as the respective default activation function and optimizer without otherwise specified. The learning rate is fixed as 0.01, the number of units at each hidden layer is set as 64, and three hidden layers and 200 epochs for the training stage are used by default. All of these DNN configurations have empirically demonstrated the best performance in our experiments.

All the bars and strings are made of linear elastic steel with a density of 7,850 kg/m³, a yield strength of 300 MPa, and a Young's modulus of 200 GPa. The bars are hollow, featuring an outer radius of 10 mm and an inner radius of 8 mm, while the strings have a radius of 2 mm.

A. Tensegrity D-Bar Unit

In the first experiment, we consider the D-bar unit tensegrity structure, as shown in Fig. 1.

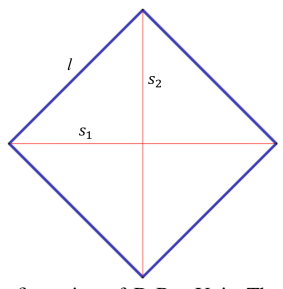


Fig. 1. Geometric configuration of D-Bar Unit. The blue and red lines are bars and strings, respectively. There are four bars and two strings in this unit. The bar length is $l=\sqrt{2}$ m.

Each data sample has two cable lengths, and the outputs consist of reduced nodal coordinates as the inputs due to the symmetry of the D-bar (only 2 coordinates), 6 member forces, and 6 non-zero frequencies. Each cable rest length change varies uniformly randomly within [-1,0] m (negative means shorten the strings). Average prediction errors in terms of average MSE for solving form-finding problems using various numbers of data samples are shown in Fig. 2.

One can observe that force errors largely dominate the overall prediction errors, decaying the fastest to 5.19×10^{-5} , while coordinate and frequency errors tend to decay more slowly or even oscillate slightly as the number of data samples increases. The average training and testing runtimes for all

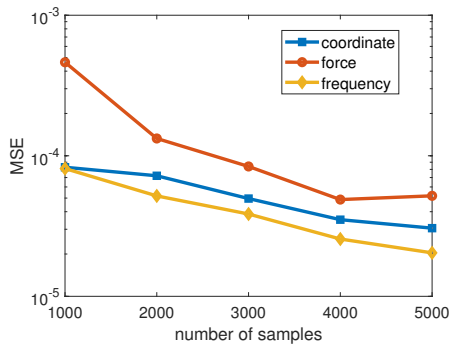


Fig. 2. Prediction errors for the D-bar dataset.

$\begin{tabular}{ll} TABLE\ I \\ RUNTIME\ FOR\ THE\ D\mbox{-bar}\ dataset. \end{tabular}$

Sample No.	1,000	2,000	3,000	4,000	5,000
Train [s]	9.15	18.65	31.75	48.78	94.62
Test [s]	11.03	23.23	36.88	48.01	62.45

the sampling cases are shown in Table I. Overall, the growth in data size leads to improved prediction accuracy, although individual components may exhibit different decay behaviors.

B. Tensegrity Prism

Next, we consider the prism tensegrity structure; see Fig. 3.

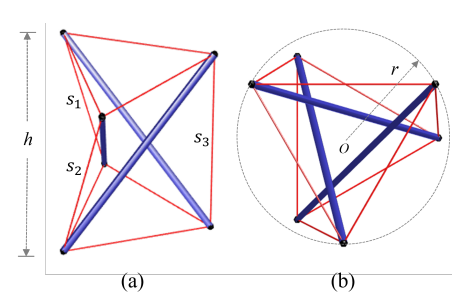


Fig. 3. Prism geometric configuration: (a) oblique view and (b) top view. The radius and height are $r=0.25~\mathrm{m}$ and $h=0.5~\mathrm{m}$.

Here, each sample consists of three cable lengths as inputs, eighteen nodal coordinates, twelve force values, and twelve non-zero frequency values as outputs. Similar to the D-bar datasets, we select the three vertical strings to change their rest length; the rest length of each cable changes within [-0.15,0] m using a uniform random sampling scheme. Average prediction errors in terms of average MSE using various numbers of samples are plotted in Fig. 4.

TABLE II
RUNTIME FOR THE PRISM DATASET.

Sample No.	1,000	2,000	3,000	4,000	5,000
Train [s]	9.23	17.45	25.16	52.17	107.22
Test [s]	11.15	22.60	34.53	50.47	68.39

One can observe that frequency errors dominate the overall prediction errors, decaying the fastest to 1.54×10^{-5} , while

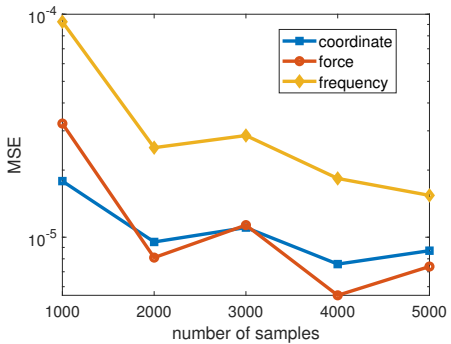


Fig. 4. Prediction errors for the prism dataset.

the decays of force and coordinate errors are very slow or even stable. The training and testing runtimes for all the sampling cases are presented in Table II. Overall, as the number of data samples increases, the overall prediction error decreases, although some components behave differently.

C. Tensegrity Lander

In the third experiment, we investigate a six-bar tensegrity lander, as shown in Fig. 5.

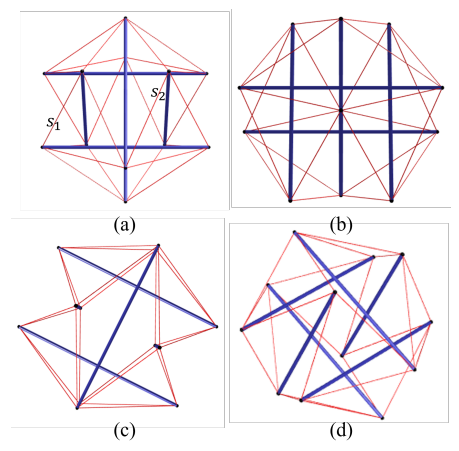


Fig. 5. Six-bar tensegrity lander geometric configuration: (a) front view, (b) side view, (c) top view, and (d) oblique view. The bar length is 1 m.

Each data sample consists of 2 cable lengths, 36 free nodal coordinates corresponding to 12 nodes, 30 member forces, and 30 non-zero frequencies. In other words, there are two inputs and 96 outputs for the DNN. The selections of cable lengths are similar to the D-bar datasets; we select two adjacent strings to change their rest length, and the rest length of each cable changes within [-0.3, 0] m using a uniform random sampling scheme.

TABLE III
RUNTIME FOR THE LANDER DATASET.

Sample No.	1,000	2,000	3,000	4,000	5,000
Train [s]	78.84	154.63	239.59	381.19	572.22
Test [s]	13.38	26.22	46.50	63.19	80.33

The average prediction errors in terms of average MSE for this dataset are shown in Fig. 6, which indicates the frequency

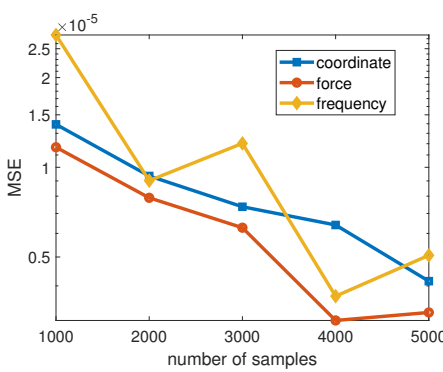


Fig. 6. Prediction errors for the lander dataset.

error dominates the entire error with a similar pattern as the prism but can achieve higher accuracy $(5.07 \times 10^{-6} \text{ compared})$ to 1.54×10^{-5}). The runtimes for the training and testing are reported in Table III. As the number of data samples increases, both the training and testing times grow while the prediction accuracy improves. Compared to the D-bar and prism datasets, the lander dataset achieves a higher prediction accuracy with the same number of data samples. This difference can be attributed to the lander dataset having a much larger number of outputs compared to the other datasets.

V. Conclusion

This paper introduces a DNN-based method to learn and predict the form-finding and physical properties of any tensegrity structures in equilibrium. Initially, we present the analytical equations governing these structures, addressing statics that include nodal coordinates and member forces, as well as natural frequencies. We then propose to train DNN models that can predict both tensegrity forms and physical properties without explicitly solving the equilibrium equations. To validate our approach, we examine three tensegrity structures: a D-bar, prism, and lander. The results indicate that: (1) The proposed approach achieves low output errors, demonstrated by the MSE of forces in the lander example being less than 3.26×10^{-6} with 5,000 samples. (2) The trained DNN prediction model performs better for complex structures, as shown by the decreasing MSE from the simpler 2D D-Bar to the more complex 3D prism and lander. (3) Increasing the sample size enhances the DNN's accuracy, evidenced by the reduction in coordinate MSE in the lander from 1.39×10^{-5} with 1,000 samples to 4.15×10^{-6} with 5,000 samples. (4) The MSE for coordinates, forces, and frequencies are all within the same order of magnitude. This technique is versatile, applicable to various tensegrity structures, and extendable to other areas of structural physics for information identification.

REFERENCES

- Robert E Skelton and Mauricio C de Oliveira, Tensegrity systems, vol. 1, Springer, 2009.
- [2] Muhao Chen, Xiaolong Bai, and Robert E Skelton, "Minimal mass design of clustered tensegrity structures," *Computer Methods in Applied Mechanics and Engineering*, vol. 404, pp. 115832, 2023.

- [3] Tara Habibi, Landolf Rhode-Barbarigos, and Thomas Keller, "Effects of prestress implementation on self-stress state in large-scale tensegrity structure," *Engineering Structures*, vol. 288, pp. 116222, 2023.
- [4] Ningning Song, Mengru Zhang, Fei Li, Ziyun Kan, Jian Zhao, and Haijun Peng, "Dynamic research on winding and capturing of tensegrity flexible manipulator," *Mechanism and Machine Theory*, vol. 193, pp. 105554, 2024.
- [5] Yuling Shen, Muhao Chen, and Robert E Skelton, "Markov data-based reference tracking control to tensegrity morphing airfoils," *Engineering Structures*, vol. 291, pp. 116430, 2023.
- [6] Ada Amendola, Anastasiia Krushynska, Mariella De Piano, Chiara Daraio, Nicola M Pugno, and Fernando Fraternali, "Mechanical modeling of the bandgap response of tensegrity metamaterials," in AIP Conference Proceedings. AIP Publishing, 2019, vol. 2116, p. 5.
- [7] Bingxing Chen and Hongzhou Jiang, "Swimming performance of a tensegrity robotic fish," *Soft robotics*, vol. 6, no. 4, pp. 520–531, 2019.
- [8] Davide Zappetti, Yi Sun, Matthieu Gevers, Stefano Mintchev, and Dario Floreano, "Dual stiffness tensegrity platform for resilient robotics," Advanced Intelligent Systems, vol. 4, no. 7, pp. 2200025, 2022.
- [9] Muhao Chen, Aguinaldo Fraddosio, Andrea Micheletti, Gaetano Pavone, Mario Daniele Piccioni, and Robert E Skelton, "Analysis of clustered cable-actuation strategies of v-expander tensegrity structures," *Engineering Structures*, vol. 296, pp. 116868, 2023.
- [10] Ryota Kobayashi, Hiroyuki Nabae, Gen Endo, and Koichi Suzumori, "Soft tensegrity robot driven by thin artificial muscles for the exploration of unknown spatial configurations," *IEEE Robotics and Automation Letters*, vol. 7, no. 2, pp. 5349–5356, 2022.
- [11] Cole Woods and Vishesh Vikas, "Design and modeling framework for dexter: Dexterous continuum tensegrity manipulator," *Journal of Mechanisms and Robotics*, vol. 15, no. 3, pp. 031006, 2023.
- [12] Luyang Zhao, Yijia Wu, Wenzhong Yan, Weishu Zhan, Xiaonan Huang, Joran Booth, Ankur Mehta, Kostas Bekris, Rebecca Kramer-Bottiglio, and Devin Balkcom, "Starblocks: Soft actuated self-connecting blocks for building deformable lattice structures," *IEEE Robotics and Automa*tion Letters, 2023.
- [13] Kenneth D Snelson, "Continuous tension, discontinuous compression structures," Feb. 16 1965, US Patent 3,169,611.
- [14] AG Tibert and Sergio Pellegrino, "Review of form-finding methods for tensegrity structures," *International Journal of Space Structures*, vol. 26, no. 3, pp. 241–255, 2011.
- [15] Rene Motro, "Tensegrity systems: the state of the art," *International journal of space structures*, vol. 7, no. 2, pp. 75–83, 1992.
- [16] Yafeng Wang, Xian Xu, and Yaozhi Luo, "Form-finding of tensegrity structures via rank minimization of force density matrix," *Engineering Structures*, vol. 227, pp. 111419, 2021.
- [17] Jingfeng He, Yihang Wang, Xin Li, Hongzhou Jiang, and Zhengmao Ye, "A modified dynamic relaxation form-finding method for general tensegrity structures with inextensible tensile members," *Computers & Structures*, vol. 291, pp. 107204, 2024.
- [18] Xing-Fei Yuan, Shuo Ma, and Shu-Hui Jiang, "Form-finding of tensegrity structures based on the levenberg-marquardt method," *Computers & Structures*, vol. 192, pp. 171–180, 2017.
- [19] Wenru Dong, Peter J Stafford, and Ana M Ruiz-Teran, "Inverse form-finding for tensegrity structures," *Computers & Structures*, vol. 215, pp. 27–42, 2019.
- [20] Seunghye Lee, Qui X Lieu, Thuc P Vo, and Jaehong Lee, "Deep neural networks for form-finding of tensegrity structures," *Mathematics*, vol. 10, no. 11, pp. 1822, 2022.
- [21] Eduard Zalyaev, Sergei Savin, and Lyudmila Vorochaeva, "Machine learning approach for tensegrity form finding: Feature extraction problem," in 2020 4th Scientific School on Dynamics of Complex Networks and their Application in Intellectual Robotics (DCNAIR). IEEE, 2020, pp. 265–268.
- [22] Kyunam Kim, Adrian K Agogino, Aliakbar Toghyan, Deaho Moon, Laqshya Taneja, and Alice M Agogino, "Robust learning of tensegrity robot control for locomotion through form-finding," in 2015 IEEE/RSJ international conference on intelligent robots and systems (IROS). IEEE, 2015, pp. 5824–5831.
- [23] Shuo Ma, Muhao Chen, and Robert E Skelton, "Dynamics and control of clustered tensegrity systems," *Engineering Structures*, vol. 264, pp. 114391, 2022.
- [24] François Chollet, "Keras," https://keras.io, 2015.
- [25] Diederik P Kingma and Jimmy Ba, "Adam: A method for stochastic optimization," arXiv preprint arXiv:1412.6980, 2014.